Intrusion tip velocity controls the emplacement mechanism of sheet intrusions

Jonas Köpping[1,2], Alexander R. Cruden[2], Samuel T. Thiele[3], Craig Magee[4], and Andrew Bunger[5,6]

[1] Department of Earth Sciences, ETH Zurich, 8092 Zurich, Switzerland

[2] School of Earth, Atmosphere and Environment, Monash University, Melbourne, 3800, Australia

[3] Helmholtz-Institute Dresden-Rossendorf, Institute Freiberg for Resource Technology, Freiberg, Germany

[4] School of Earth and Environment, University of Leeds, Leeds, LS2 9JT, UK

[5] Department of Civil and Environmental Engineering, University of Pittsburgh, Pittsburgh, PA 15269, USA

[6] Department of Chemical and Petroleum Engineering, University of Pittsburgh, Pittsburgh, PA 15269, USA

ABSTRACT

Space for intruding magma is created by elastic, viscous, and/or plastic deformation of host rocks. Such deformation impacts the geometries of igneous intrusions, particularly sills and dikes. For example, tapered intrusion tips indicate linear-elastic fracturing during emplacement, whereas fluidization of host rocks has been linked to development of elongate magma fingers with rounded tips. Although host rock fluidization has only been observed at the lateral tips of magma fingers, it is assumed to occur at their leading edges (frontal tips), and thereby control their propagation

and geometry. Here, we present macro- and microstructural evidence of fluidized sedimentary host rock at the lateral tips of magma fingers emanating from the Shonkin Sag laccolith (Montana, USA), and explore whether fluidization could have occurred at their frontal tips. Specifically, we combine heat diffusion modelling and fracture tip velocity estimates to show that: (i) low intrusion tip velocities ($\leq 10^{-5}$ m s^{-1}) allow pore fluids ahead of the intrusion to reach temperatures sufficient to cause fluidization; but (ii) when tip velocities are high (~0.01–1 m s^{-1}), typical for many sheet intrusions, fluidization ahead of propagating tips is inhibited. Our results suggest that intrusion tip velocity (i.e., strain rate) is a first-order control on how rocks accommodate magma. Spatially and temporarily varying velocities of lateral and frontal tips suggests deformation mechanisms at these sites may be decoupled, meaning magma finger formation may not require host rock fluidization. It is thus critical to consider strain rate and 3D intrusion geometry when inferring dominant magma emplacement mechanisms.

INTRODUCTION

Igneous sheet intrusions (dikes and sills) often develop via the amalgamation of smaller building blocks, here called "elements" (e.g., Pollard et al., 1975, 1982; Schofield et al., 2012; Wilson et al., 2016; Köpping et al., 2022). Some elements have finger-like (or pipe-like) geometries, with cross-sectional thickness-to-width ratios of ~0.1–1, which either coalesce into a continuous sheet or propagate as isolated structures (Fig. 1A). Understanding the initiation and propagation of these specific elements, often termed *magma fingers*, is important because they can control magma flow localization (e.g., Köpping et al., 2023). Such localization of flow can impact magma storage and eruption sites (e.g., Cashman and Sparks, 2013), and contribute to the accumulation of

45 orthomagmatic Ni-Cu-PGE sulphide deposits, which are often hosted in elongate, pipe-like
46 intrusions (e.g., Barnes et al., 2016).
47 Evidence for the disaggregation of host rocks by fluidization is often observed adjacent to the
48 *lateral* tips of finger-like elements (Fig. 1), which led to the interpretation that magma fingers form
49 by viscous fingering instabilities (Pollard et al., 1975; Schofield et al., 2010). However, as *frontal*
50 magma finger tips are rarely exposed in nature, we have to rely on modelling to test whether
51 fluidization can also occur at and drive the propagation of frontal magma finger tips. Here, we
52 combine structural field observations of lateral magma finger tips from the outer margin of the
53 Shonkin Sag laccolith (Montana, USA), with thermal modelling to evaluate whether the observed
54 deformation is analogous to that at unexposed frontal tips. Specifically, we assess whether host
55 rocks ahead of a propagating sheet intrusion can undergo significant fluidization to initiate the
56 formation of magma fingers (Schofield et al., 2010). Since dominant sheet intrusion emplacement
57 mechanisms are commonly inferred from host rock deformation observed near intrusion tips, our
58 work will further increase our knowledge on how magma migrates in the upper crust.
59

60 **SHEET INTRUSION ELEMENTS**

61 Field observations and 3D seismic reflection data indicate that element geometries range from
62 ribbon-like to pipe-like (Pollard et al., 1975, 1982; Galland et al., 2019; Stephens et al., 2021).
63 Ribbon-like elements are commonly vertically offset from each other, rotated about their long axis,
64 and associated with tensile-brittle magma emplacement (i.e., fracturing; e.g., Hutton, 2009;
65 Schofield et al., 2012; Magee et al., 2019; Stephens et al., 2021). In contrast, pipe-like elements
66 are often attributed to non-brittle magma emplacement mechanisms (e.g., Schofield et al., 2012).
67 Pollard et al. (1975) first coined the term *finger* or *magma finger* to describe pipe-like intrusions

that are exposed on the margin of the Shonkin Sag laccolith (Fig. 1), and suggested they formed in response to the development of viscous instabilities at the magma–host rock contact. Specifically, Pollard et al. (1975) related magma fingers to the phenomenon of viscous fingering, which describes the unstable displacement of a high-viscosity fluid (i.e., fluidized host rock) by one of a lower viscosity (i.e., magma; Saffman and Taylor, 1958). Such viscous fingering may occur during: (i) intrusion-induced heating of local pore fluids, which increases their fluid pressure beyond the brittle strength of the host rock (e.g., Kokelaar, 1982; Schofield et al., 2010); or (ii) when secondary processes, such as overburden failure, cause a rapid pressure drop in the host rock pore fluids (Schofield et al., 2010). These conditions can lead to boiling or flash boiling of the pore fluids, respectively, driving their explosive expansion and disaggregating the sedimentary host rock such that it can behave as a high viscosity fluid (e.g., Kokelaar, 1982; Schofield et al., 2010). Evidence for such *thermal* and *triggered* host rock fluidization has been observed at the lateral tips, and the top and bottom contacts of numerous sheet intrusions and magma fingers, but not their frontal tips (e.g., Kokelaar, 1982; Schofield et al., 2010, 2012).

GEOLOGICAL AND STRUCTURAL OBSERVATIONS

The Shonkin Sag laccolith, located in the Highwood Mountains, MT, USA, formed at ca. 50 Ma at a depth of ~1.4 km and consists of mafic shonkinite and syenite (Barksdale, 1937; Marvin et al., 1980). The laccolith was emplaced into the tectonically undeformed Eagle Sandstone Formation, a fine-grained Cretaceous sandstone with thin shale interbeds (Pollard et al., 1975). Five shonkinite sills emerge from the SE margin of the laccolith and are well exposed along a ~1.8 km long, E-W trending cliff face. These sills show evidence of coalesced and isolated m-scale magma fingers,

which propagated towards the SE along the sub-horizontal host rock bedding (Fig. 1B; Pollard et al., 1975).

In cross sections oblique to the magma finger long axes, fingers at the SE margin of the Shonkin Sag laccolith are 0.5–1.3 m thick and 1–13 m wide, with aspect ratios of 0.1–0.85 (Fig. 1B). In addition to folding and shearing of host rock strata between magma fingers (Pollard et al., 1975), evidence of host rock fluidization is commonly observed (Figs. 1B, 2). Specifically, juvenile clasts of shonkinite mingle with sedimentary host rock to form *peperite* around lateral finger tips (Figs. 1B, 2). Irregularly-shaped fluidal clast morphologies indicate shearing between fluidized host rock and intruding magma (Fig. 2; e.g., Skilling et al., 2002). These fluidal clasts are observed ≤1 m from the exposed lateral finger tips (Fig. 2A). At the micro-scale, fragments of originally continuous, flat-lying shale interlayers (<1 cm thick) are dispersed and rotated within the peperite, and they are crosscut locally by tensile fractures that do not extend into the sandstone matrix (Fig. 2B, i). Isolated quartz and feldspar grains float within a calcite and dolomite matrix, indicating further evidence for host rock fluidization and mobilization (Fig. 2B, ii). Together, these observations indicate that the sandstone was fluidized at the dm- to m-scale adjacent to the lateral finger tips.

ROLE OF INTRUSION TIP VELOCITY

Field observations and numerical models of magma fingers are commonly limited to 2D lateral tips (e.g., Pollard et al., 1975; Schofield et al., 2012; Souche et al., 2019; Stephens et al., 2021). Despite this limitation, such data and models are used to infer finger formation and frontal propagation mechanisms (e.g., Schofield et al., 2010, 2012; Spacapan et al., 2017). Here, we use heat transfer modelling and fracture tip velocity estimates to constrain the conditions under which

host rock fluidization can occur. These calculations allow us to assess whether host rock fluidization can initiate viscous fingering ahead of a propagating sheet intrusion.

Fluidization ahead of a propagating sill tip requires sufficient heat transfer to cause pore fluid boiling ahead of the intrusion (e.g., Kokelaar, 1982; Schofield et al., 2010). Considering heat transfer by thermal diffusion and, for simplicity, assuming negligible convective heat transfer, the characteristic length (L_d) of heat diffusion ahead of an intrusion tip is:

$$L_d = \sqrt{\kappa t} \quad \text{(Eq. 1)},$$

where κ = thermal diffusion ($m^2\ s^{-1}$) and t = time (s) (Turcotte and Schubert, 2002). If L_d is greater than the distance travelled by the intrusion tip ($L_{adv} = Ut$), moving at velocity U ($m\ s^{-1}$), heat from the intruding magma diffuses into the host rocks at rates faster than tip propagation, and pore fluids ahead of the propagating tip may reach temperatures sufficient for boiling to occur. The temperature ahead of the intrusion, T, is then approximated by:

$$T = T_\infty + (T_m - T_\infty)e^{-\frac{U}{\kappa}L} \quad \text{(Eq. 2)},$$

where T_∞ = background temperature (e.g., 52.5 ºC at 1500 m depth), T_m = magma temperature (1000–1200 ºC for mafic magmas), and L = distance (m) ahead of the intrusion tip (Fig. 3A; Supplemental Material 1; Turcotte and Schubert, 2002). For a reasonable value of κ for sandstone ($1.3 \times 10^{-6}\ m^2\ s^{-1}$; Geng et al., 2018), sill tip velocities between 10^{-5} and $10^{-6}\ m\ s^{-1}$ will heat pore fluids to 300–350 ºC within a distance of ~0.15 to 1.5 m ahead of the propagating intrusion, respectively (Fig. 3B). These temperatures are sufficient to cause boiling at depths of 1–2 km (Kokelaar, 1982), potentially fluidizing the sandstone and allowing viscous finger formation or growth. Higher tip velocities ($\geq 10^{-4}\ m\ s^{-1}$) only allow boiling (T≥350 ºC) within ≤1.5 cm or flash boiling (T≥100 ºC) triggered by tensile host rock failure within ≤3.5 cm ahead of the intrusion (Fig. 3B), which we consider insufficient to initiate meter-scale magma fingers. Our thermal

136 modelling approach assumes a constant heat source and represents the upper bound to heat transfer.
137 The results indicate that thermal and triggered host rock fluidization are only likely to occur when
138 intrusion tip velocities are low ($\leq 10^{-5}$ m s^{-1}), which contrasts with high tip velocities of up to 1 m
139 s^{-1} assumed in previous studies (Schofield et al., 2010).
140 Because our calculations suggest fluidization requires low intrusion tip velocities, it is useful to
141 mechanistically bound the tip velocities based on measured apertures of fluid-driven fractures,
142 assuming linear-elastic fracturing as initial emplacement mechanism (e.g., Gudmundsson, 2011).
143 For the case where the tip advance is driven by a viscous fluid and the host rock is elastic, the tip
144 velocity (V) of a hydro-fracture propagating in a regime where the dynamics are determined by
145 the viscosity of the fracture fluid is approximated by:
146 $$V \sim \frac{E' w^3}{216 * \sqrt{3} * \mu s^2} \quad \text{(Eq. 3)},$$
147 where E'= plane strain modulus, μ = fluid viscosity, w = fracture opening, and s = distance
148 between w-measurement and the fracture tip (Fig. 3C; Desroches et al., 1994; Detournay, 2016;
149 Xing et al., 2017). To approximate intrusion tip velocities, we use field constraints for w and s
150 from sills and dikes with sharp tip geometries, which suggest propagation via linear-elastic
151 fracturing (Supplemental Material 1, 2; Galland et al., 2018; Poppe et al., 2020; Schmiedel et al.,
152 2021; Walker et al., 2021). Using this approach, low tip velocities ($<10^{-5}$ m s^{-1}) required to cause
153 pore fluid boiling and host rock fluidization can be achieved by high-viscosity ($\mu \geq 10^8$ Pa s) felsic
154 or crystal-rich magmas, but not by low-viscosity mafic magmas such as shonkinite (Fig. 3D;
155 Murase and McBirney, 1973).
156
157 **DISCUSSION AND CONCLUSIONS**

158 Frequent observations of fluidized host rock in the vicinity of magma fingers may support an
159 interpretation linking fluidization and magma finger formation via viscous instabilities (Pollard et
160 al. 1975; Schofield et al., 2010, 2012). However, our modelling suggests that host rocks will not
161 undergo fluidization when the magma propagation velocity is representative of laterally
162 propagating sheet intrusions (~0.01–1 m s^{-1}; e.g., Ágústsdóttir et al., 2016). The initiation of
163 magma fingers may therefore not be due to viscous fingering caused by host rock fluidization.
164 Instead, we hypothesize that the fluidized host rocks observed adjacent to magma fingers are linked
165 to the different propagation velocities between frontal versus lateral tips (Fig. 4). Variable stress
166 accumulation at intrusion tips (Walker et al., 2021), local changes in emplacement conditions such
167 as natural variations in pore fluid content and host rock matrix strength (Stephens et al., 2021), or
168 overlapping temperature halos of adjacent magma fingers may explain the irregular occurrence of
169 fluidization in the vicinity of magma fingers (Fig. 1B) and may affect host rock deformation.
170 Critically, the elongate 3D geometry of magma fingers implies higher velocity (i.e., higher strain
171 rate) at the frontal tips, causing lengthening, and lower velocity (i.e., lower strain rate) at lateral
172 tips, causing finger widening and coalescence (Fig. 4A), which has been confirmed by 3D
173 laboratory experiments (Arachchige et al., 2022). Lateral finger tips are therefore unlikely to
174 propagate by the same mechanism as frontal tips. Linking magma fingers to potential high strain
175 rate regimes will contribute to unravelling their initiation and propagation mechanisms, and as
176 such to better understanding the formation of orthomagmatic Ni-Cu-PGE deposits, which are often
177 hosted in mafic and ultramafic, elongate or pipe-like intrusions in which magma flow can
178 channelize (Barnes et al., 2016).
179 Overall, we suggest that low velocity propagation, associated with low strain rates, and a
180 continuous heat supply, combined with local stress accumulation at lateral finger tips make these

favorable sites for host rock fluidization (Fig. 4B). Deformation features observed at lateral tips therefore reflect intrusion widening and vertical inflation rather than finger formation or lengthening, from which they are decoupled spatially and temporally due to the differences in strain rates and thermal regimes. Tip velocity and strain rate are thus key, but largely ignored, parameters that control how host rocks accommodate magma emplacement. As the tip velocity of elements (e.g., fingers), or entire sheet intrusions, varies spatially along their edges (e.g., frontal tip velocities of bladed dikes or elongate sills are faster than their lateral tips; Townsend et al., 2017; Davis et al., 2021), interpreting magma emplacement mechanisms based on 2D outcrop observations may not fully capture all the processes accommodating emplacement. Furthermore, our findings suggest magma emplacement mechanisms could be temporally variable throughout their lifespan, requiring caution when inferring dominant magma emplacement mechanisms in the upper crust from final intrusion forms and associated host rock deformation.

ACKNOWLEDGEMENTS

We are grateful to Mr. and Mrs. Ebeling for permitting access to the cliff faces of the Shonkin Sag laccolith. We thank Anja Slim for her support with heat diffusion modelling and Richard Walker for providing photographs of sill tips. We gratefully acknowledge helpful reviews from Penelope Wilson, Steffi Burchardt, and an anonymous reviewer, and we thank Robert Holdsworth for his editorial handling of the manuscript. JK was supported by a Monash Graduate Scholarship and a Graduate Research Completion Award. ARC and CM were supported by Australian Research Council Discovery Grant DP190102422.

REFERENCES

Ágústsdóttir, T., Woods, J., Greenfield, T., Green, R.G., White, R.S., Winder, T., Brandsdóttir, B., Steinthórsson, S., and Soosalu, H., 2016, Strike-slip faulting during the 2014 Bárðarbunga-Holuhraun dike intrusion, central Iceland: Geophysical Research Letters, v. 43, p. 1495–1503, doi:10.1002/2015GL067423.

Arachchige, U.N., Cruden, A.R., Weinberg, R., Slim, A., and Köpping, J., 2022, Saucers, Fingers, and Lobes: New Insights on Sill Emplacement From Scaled Laboratory Experiments: Journal of Geophysical Research: Solid Earth, v. 127, p. e2022JB024421, doi:10.1029/2022JB024421.

Barksdale, J.D., 1937, The Shonkin Sag laccolith: American Journal of Science, v. 33, p. 321–359.

Barnes, S.J., Cruden, A.R., Arndt, N., and Saumur, B.M., 2016, The mineral system approach applied to magmatic Ni–Cu–PGE sulphide deposits: Ore Geology Reviews, v. 76, p. 296–316, doi:10.1016/j.oregeorev.2015.06.012.

Cashman, K.V., and Sparks, R.S.J., 2013, How volcanoes work: A 25 year perspective: Bulletin of the Geological Society of America, v. 125, p. 664–690, doi:10.1130/B30720.1.

Davis, T., Bagnardi, M., Lundgren, P., and Rivalta, E., 2021, Extreme Curvature of Shallow Magma Pathways Controlled by Competing Stresses: Insights From the 2018 Sierra Negra Eruption: Geophysical Research Letters, v. 48, p. e2021GL093038, doi:10.1029/2021GL093038.

Desroches, J., Detournay, E., Lenoach, B., Papanastasiou, P., Pearson, J.P.A., Thiercelin, M., and Cheng, A., 1994, The crack tip region in hydraulic fracturing: Proceedings of the Royal Society of London. Series A: Mathematical and Physical Sciences, v. 447, p. 39–48, doi:10.1098/rspa.1994.0127.

Detournay, E., 2016, Mechanics of Hydraulic Fractures: Annual Review of Fluid Mechanics, v. 48, p. 311–339, doi:10.1146/annurev-fluid-010814-014736.

Galland, O. et al., 2018, Storage and Transport of Magma in the Layered Crust—Formation of Sills and Related Flat-Lying Intrusions, *in* Volcanic and Igneous Plumbing Systems, Elsevier, p. 113–138, doi:10.1016/B978-0-12-809749-6.00005-4.

Galland, O., Spacapan, J.B., Rabbel, O., Mair, K., Soto, F.G., Eiken, T., Schiuma, M., and Leanza, H.A., 2019, Structure, emplacement mechanism and magma-flow significance of igneous fingers – Implications for sill emplacement in sedimentary basins: Journal of Structural Geology, v. 124, p. 120–135, doi:10.1016/j.jsg.2019.04.013.

Geng, J., Sun, Q., Zhang, Y., Cao, L., Lü, C., and Zhang, Y., 2018, Temperature dependence of the thermal diffusivity of sandstone: Journal of Petroleum Science and Engineering, v. 164, p. 110–116, doi:10.1016/j.petrol.2018.01.047.

Gudmundsson, A., 2011, Rock Fractures in Geological Processes: Cambridge, New York, Cambridge University Press, 1–569 p.

Hutton, D.H.W., 2009, Insights into magmatism in volcanic margins: bridge structures and a new mechanism of basic sill emplacement - Theron Mountains, Antarctica: Petroleum Geoscience, v. 15, p. 269–278, doi:10.1144/1354-079309-841.

Kokelaar, B.P., 1982, Fluidization of wet sediments during the emplacement and cooling of various igneous bodies: Journal of the Geological Society, v. 139, p. 21–33, doi:10.1144/gsjgs.139.1.0021.

Köpping, J., Cruden, A.R., Magee, C., McCarthy, W., Geissman, J., and Holm, D., 2023, Magnetic fabrics reveal three-dimensional flow processes within elongate magma fingers at the margin of the Shonkin Sag laccolith (MT, USA): Journal of Structural Geology, v. 169, p. 104829, doi:10.1016/j.jsg.2023.104829.

Köpping, J., Magee, C., Cruden, A.R., Jackson, C.A.-L., and Norcliffe, J.R., 2022, The building blocks of igneous sheet intrusions: Insights from 3-D seismic reflection data: Geosphere, doi:10.1130/GES02390.1.

Magee, C., Muirhead, J., Schofield, N., Walker, R.J., Galland, O., Holford, S., Spacapan, J., Jackson, C.A.L., and McCarthy, W., 2019, Structural signatures of igneous sheet intrusion propagation: Journal of Structural Geology, v. 125, p. 148–154, doi:10.1016/j.jsg.2018.07.010.

Marvin, R.F., Hearn Jr., B.O., Mehnert, H.H., Naesser, C.W., Zartman, R.E., and Lindsley, D.A., 1980, Late Cretaceous-Paleocene igneous activity in north-central Montana: Isochron/West, v. 29, p. 5–25.

Murase, T., and McBirney, A.R., 1973, Properties of Some Common Igneous Rocks and Their Melts at High Temperatures: Geological Society of America Bulletin, v. 84, p. 3563, doi:10.1130/0016-7606(1973)84<3563:POSCIR>2.0.CO;2.

Pollard, D.D., Muller, O.H., and Dockstader, D.R., 1975, The form and growth of fingered sheet intrusions: Geological Society of America Bulletin, v. 86, p. 351–363, doi:10.1130/0016-7606(1975)86<351:TFAGOF>2.0.CO;2.

Pollard, D.D., Segall, P., and Delaney, P.T., 1982, Formation and interpretation of dilatant echelon cracks.: Geological Society of America Bulletin, v. 93, p. 1291–1303, doi:10.1130/0016-7606(1982)93<1291:FAIODE>2.0.CO;2.

Poppe, S., Galland, O., de Winter, N.J., Goderis, S., Claeys, P., Debaille, V., Boulvais, P., and Kervyn, M., 2020, Structural and Geochemical Interactions Between Magma and Sedimentary Host Rock: The Hovedøya Case, Oslo Rift, Norway: Geochemistry, Geophysics, Geosystems, v. 21, p. 1–22, doi:10.1029/2019GC008685.

Saffman, P.G., and Taylor, G.I., 1958, The penetration of a fluid into a porous medium or Hele-Shaw cell containing a more viscous liquid: Dynamics of Curved Fronts, v. 245, p. 312–329, doi:10.1016/B978-0-08-092523-3.50017-4.

Schmiedel, T., Burchardt, S., Mattsson, T., Guldstrand, F., Galland, O., Palma, J., and Skogby, H., 2021, Emplacement and Segment Geometry of Large, High-Viscosity Magmatic Sheets: Minerals, v. 11, p. 1113, doi:10.3390/min11101113.

Schofield, N.J., Brown, D.J., Magee, C., and Stevenson, C.T., 2012, Sill morphology and comparison of brittle and non-brittle emplacement mechanisms: Journal of the Geological Society, v. 169, p. 127–141, doi:10.1144/0016-76492011-078.

Schofield, N.J., Stevenson, C., and Reston, T., 2010, Magma fingers and host rock fluidization in the emplacement of sills: Geology, v. 38, p. 63–66, doi:10.1130/G30142.1.

Skilling, I.P., White, J.D.L., and McPhie, J., 2002, Peperite: A review of magma-sediment mingling: Journal of Volcanology and Geothermal Research, v. 114, p. 1–17, doi:10.1016/S0377-0273(01)00278-5.

Souche, A., Galland, O., Haug, Ø.T., and Dabrowski, M., 2019, Impact of host rock heterogeneity on failure around pressurized conduits: Implications for finger-shaped magmatic intrusions: Tectonophysics, v. 765, p. 52–63, doi:10.1016/j.tecto.2019.05.016.

Spacapan, J.B., Galland, O., Leanza, H.A., and Planke, S., 2017, Igneous sill and finger emplacement mechanism in shale-dominated formations: a field study at Cuesta del Chihuido, Neuquén Basin, Argentina: Journal of the Geological Society, v. 174, p. 422–433, doi:10.1144/jgs2016-056.

Stephens, T., Walker, R., Healy, D., and Bubeck, A., 2021, Segment tip geometry of sheet intrusions, II: Field observations of tip geometries and a model for evolving emplacement mechanisms: Volcanica, v. 4, p. 203–225, doi:10.30909/vol.04.02.203225.

Townsend, M.R., Pollard, D.D., and Smith, R.P., 2017, Mechanical models for dikes: A third school of thought: Tectonophysics, v. 703–704, p. 98–118, doi:10.1016/j.tecto.2017.03.008.

Turcotte, D.L., and Schubert, G., 2002, Geodynamics: Cambridge University Press, v. 2.

Walker, R., Stephens, T., Greenfield, C., Gill, S., Healy, D., and Poppe, S., 2021, Segment tip geometry of sheet intrusions, I: Theory and numerical models for the role of tip shape in controlling propagation pathways: Volcanica, v. 4, p. 189–201, doi:10.30909/vol.04.02.189201.

Wilson, P.I.R., McCaffrey, K.J.W., Wilson, R.W., Jarvis, I., and Holdsworth, R.E., 2016, Deformation structures associated with the Trachyte Mesa intrusion, Henry Mountains, Utah: Implications for sill and laccolith emplacement mechanisms: Journal of Structural Geology, v. 87, p. 30–46, doi:10.1016/j.jsg.2016.04.001.

Xing, P., Yoshioka, K., Adachi, J., El-Fayoumi, A., and Bunger, A.P., 2017, Laboratory measurement of tip and global behavior for zero-toughness hydraulic fractures with circular and blade-shaped (PKN) geometry: Journal of the Mechanics and Physics of Solids, v. 104, p. 172–186, doi:10.1016/j.jmps.2017.04.013.

FIGURE CAPTIONS

Figure 1. (A) Schematic 3D diagram shows elongate magma fingers emerging from a continuous sheet. Schematic 2D cross-sections show coalesced and separate magma fingers. (B) Photograph shows cross-sectional outcrop of individual magma fingers at the outer margin of the Shonkin Sag laccolith. Magma emplacement-related host rock deformation at lateral tips is indicated in (A) and (B).

Figure 2. (A) Photograph and sketch interpretation of an oblique cross-section through a magma finger, revealing peperite adjacent to a lateral tip. Inset shows a fluidal shonkinite clast morphology. (B) Thin sections of a peperite sample scanned under crossed polarized light showing juvenile shonkinite clasts and shale fragments mingled with mobilized host rock. High-angle fractures in shale layers do not extend into the sandstone (i) and quartz and feldspar grains floating in a matrix of calcite and dolomite (ii) highlight that the sandstone was fluidized. Note that thin sections show representative examples of fluidized sandstone adjacent to the Shonkin Sag magma fingers.

Figure 3. (A, B) Temperature (T) ahead of a propagating intrusion tip, at a specific length (L) calculated for a range of sill tip velocities (U) using Eq. 2. (C, D) Fracture tip velocities (V) for a range of magma viscosities (μ) estimated using Eq. 3.

Figure 4. (A) Schematic map-view time-series shows the propagation and formation of elongate sheet intrusions (t_0) and magma fingers (t_1, t_2). Lateral and frontal intrusions tips and temperature contours are indicated. (B) Schematic block diagram highlights the difference in temperature

around frontal and lateral intrusion tips with high and low tip velocities, respectively. Regions where host rock fluidization is likely to occur are indicated.

Width: 118 mm
Height: 135 mm

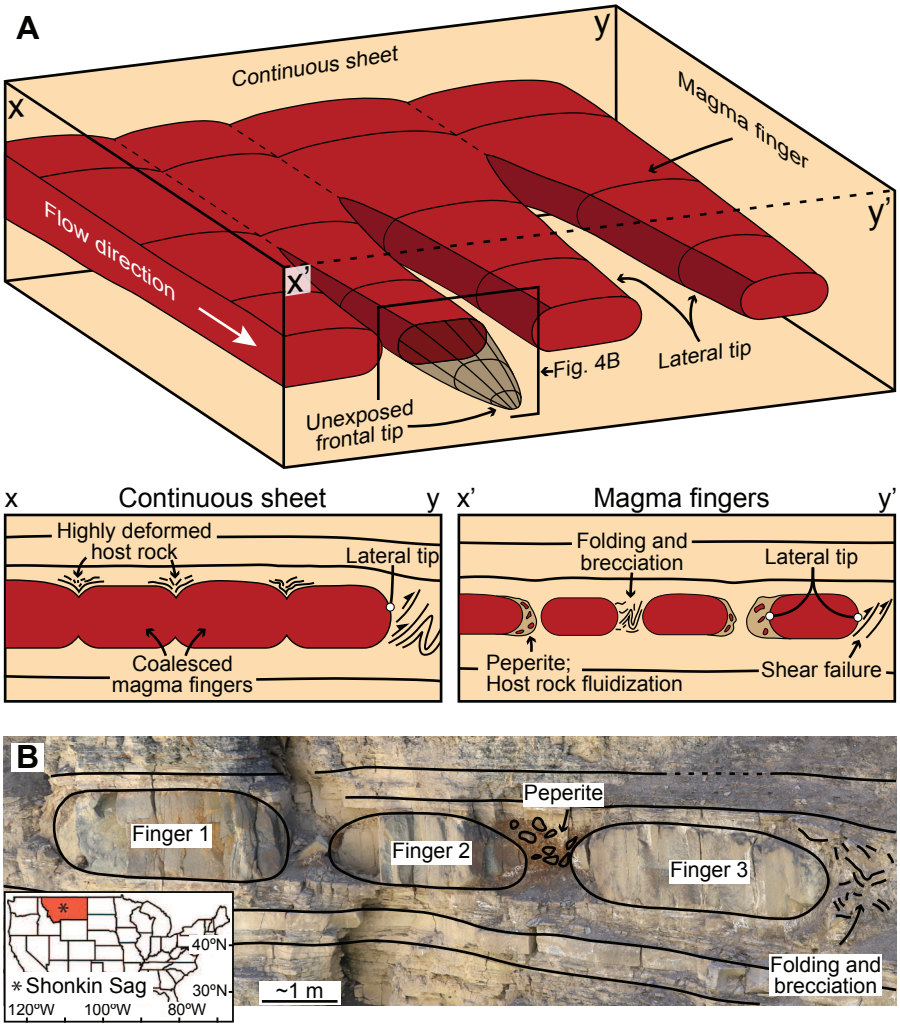

Figure 1. (A) Schematic 3D diagram shows elongate magma fingers emerging from a continuous sheet. Schematic 2D cross-sections show coalesced and separate magma fingers. (B) Photograph shows cross-sectional outcrop of individual magma fingers at the outer margin of the Shonkin Sag laccolith. Magma emplacement-related host rock deformation at lateral tips is indicated in (A) and (B).

Width: 118 mm
Height: 130 mm

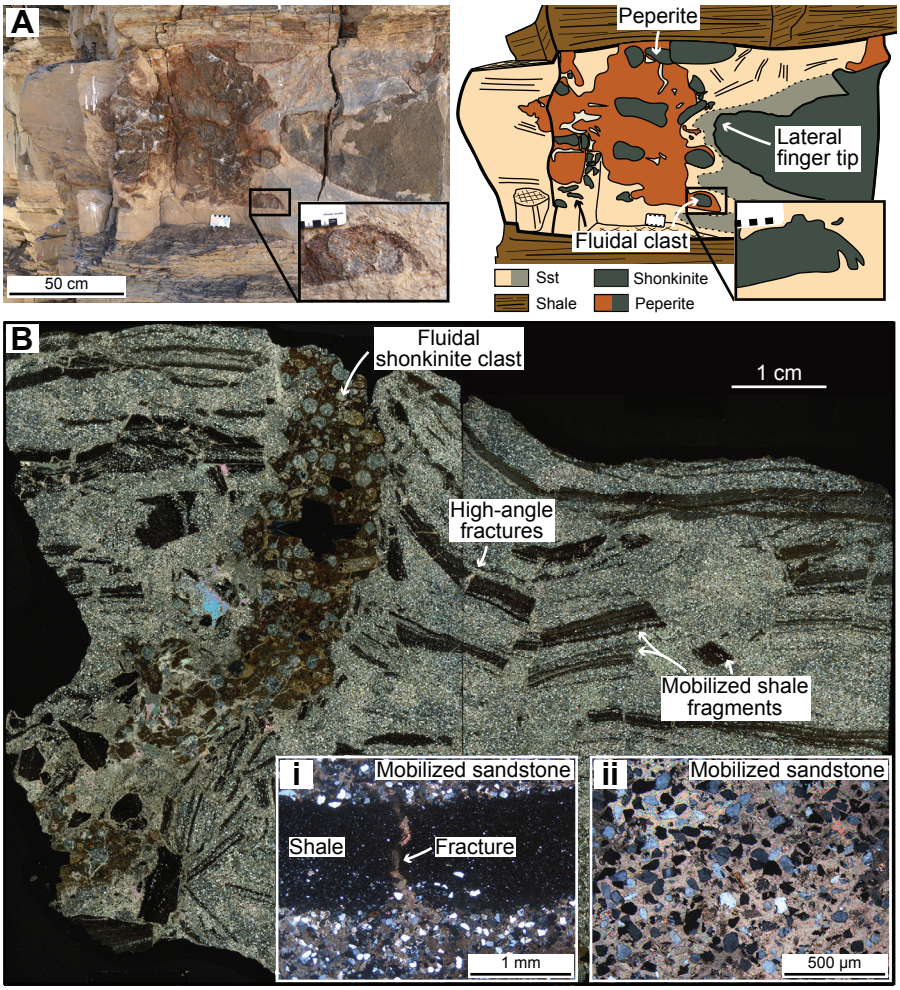

Figure 2. (A) Photograph and sketch interpretation of an oblique cross-section through a magma finger, revealing peperite adjacent to a lateral tip. Inset shows a fluidal shonkinite clast morphology. (B) Thin sections of a peperite sample scanned under crossed polarized light showing juvenile shonkinite clasts and shale fragments mingled with mobilized host rock. High-angle fractures in shale layers do not extend into the sandstone (i) and quartz and feldspar grains floating in a matrix of calcite and dolomite (ii) highlight that the sandstone was fluidized. Note that thin sections show representative examples of fluidized sandstone adjacent to the Shonkin Sag magma fingers.

Width: 177 mm
Height: 94 mm

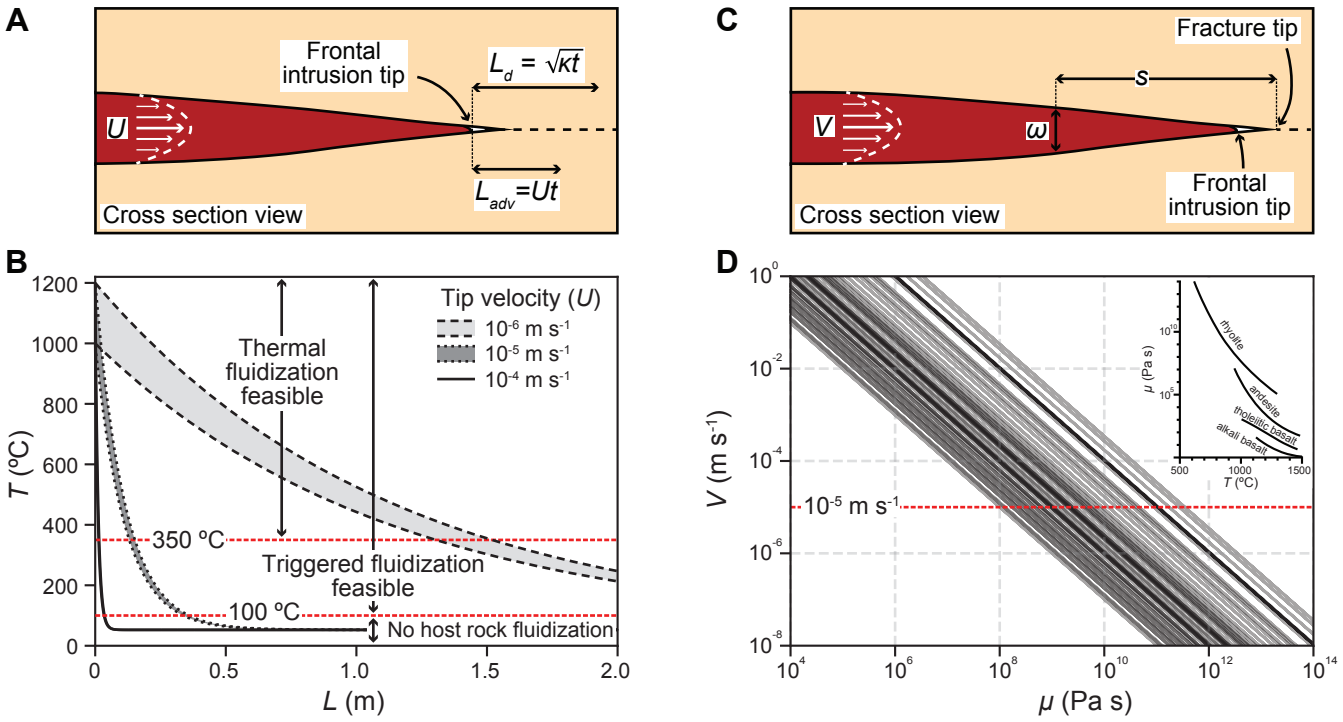

Figure 3. (A, B) Temperature (T) ahead of a propagating intrusion tip, at a specific length (L) calculated for a range of sill tip velocities (U) using Eq. 2. (C, D) Fracture tip velocities (V) for a range of magma viscosities (μ) estimated using Eq. 3.

Width: 118 mm
Height: 112 mm

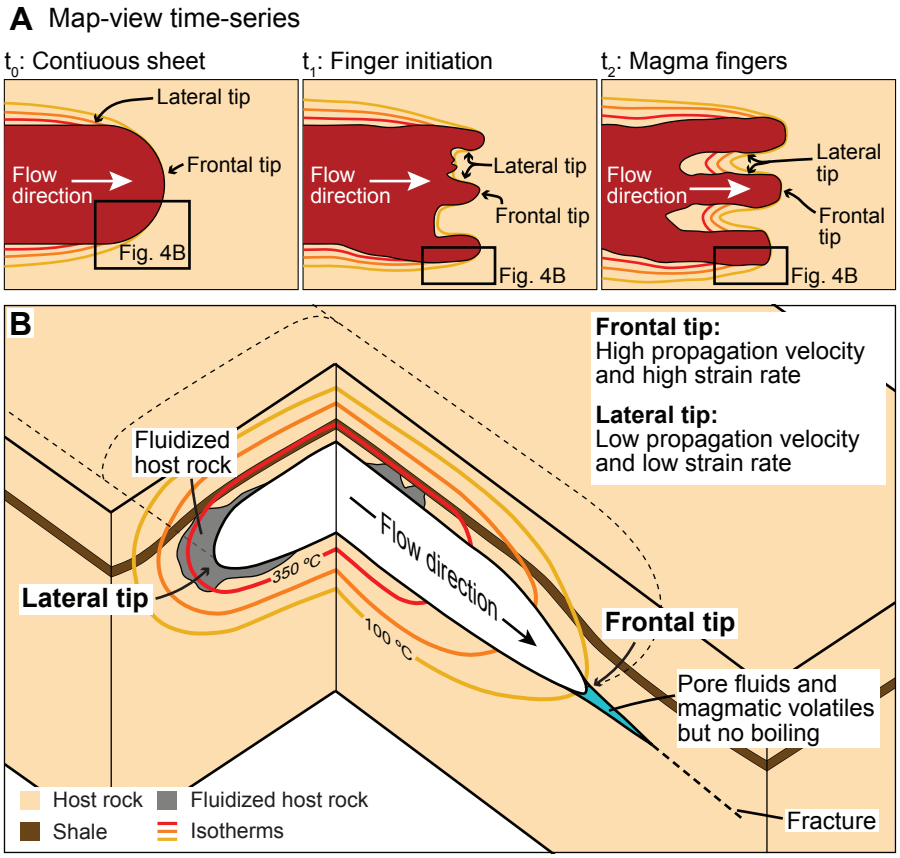

Figure 4. (A) Schematic map-view time-series shows the propagation and formation of elongate sheet intrusions (t_0) and magma fingers (t_1, t_2). Lateral and frontal intrusions tips and temperature contours are indicated. (B) Schematic block diagram highlights the difference in temperature around frontal and lateral intrusion tips with high and low tip velocities, respectively. Regions where host rock fluidization is likely to occur are indicated.